Title

Pathways of the Agulhas waters poleward of 29°S

Journal

Journal of Geophysical Research - Oceans, 119(7)

ISSN

2169-9275

Authors

Wang, Jinbo
Mazloff, Matthew R
Gille, Sarah T

Publication Date

2014-07-01

DOI

10.1002/2014jc010049

Peer reviewed

AGU PUBLICATIONS

JGR

Journal of Geophysical Research: Oceans

RESEARCH ARTICLE

10.1002/2014JC010049

Key Points:
- The pathways of Agulhas waters are mapped using passive tracer in SOSE
- Agulhas waters can be mixed into the SEISAMW and ACC
- Cross-ACC mixing is aggrandized by topography

Supporting Information:
- Description of video
- Video

Correspondence to:
J. Wang,
jinbow@alum.mit.edu

Citation:
Wang, J., M. R. Mazloff, and S. T. Gille (2014), Pathways of the Agulhas waters poleward of 29°S, *J. Geophys. Res. Oceans*, *119*, 4234–4250, doi:10.1002/2014JC010049.

Received 20 APR 2014
Accepted 12 JUN 2014
Accepted article online 14 JUN 2014
Published online 9 JUL 2014

Pathways of the Agulhas waters poleward of 29°S

Jinbo Wang[1], Matthew R. Mazloff[1], and Sarah T. Gille[1]

[1]Scripps Institution of Oceanography, UCSD, La Jolla, California, USA

Abstract Passive tracers are advected in a Southern Ocean State Estimate (SOSE) to map the pathways of Agulhas waters, with a focus on determining where the Agulhas waters intrude into the Antarctic Circumpolar Current (ACC). Results show that Agulhas waters spread into all three ocean basins within 3 years of release. After leaving the African continent, the mean Agulhas water pathway tilts northwest toward the South Atlantic and southeast toward the ACC. The majority (from 60% to 100% depending on specific water mass) of the Agulhas waters stay in the South Indian Ocean north of the Sub-Antarctic Front. From 10 to 28% enters the South Atlantic Ocean through the boundary current along the southern tip of South Africa and via Agulhas rings in the retroflection region. Up to 12% of intermediate depth Agulhas waters enter the ACC. Most of the tracer transport into the ACC occurs just downstream of the Kerguelen Plateau, which clearly demonstrates the importance of topography in elevating cross-frontal exchange. Agulhas waters also contribute to Sub-Antarctic Mode Water formation in the Southeast Indian Ocean by lateral advection. The surface Agulhas waters are preconditioned by strong surface buoyancy loss before turning into mode water, while the intermediate Agulhas waters are advected to the mode water formation region along isopycnals before being drawn into the mixed layer.

1. Introduction

The Agulhas Current, the swift boundary current along the southeast coast of the African continent, is one of the major western boundary currents in the world oceans. It carries warm and saline Indian, Arabian Sea, and Red Sea waters southward along the southeast African coast [*Harris*, 1972; *Lutjeharms*, 1976; *Biastoch and Krauss*, 1999; *Beal et al*., 2006]. It splits into two branches after passing the Agulhas bank. One branch, the so-called Agulhas leakage, transports Indian Ocean waters into the south Atlantic via energetic and intermittent Agulhas rings [*Richardson*, 2007]. This transport of warm and saline Indian water by the Agulhas leakage is referred to as the "warm water route" in the global conveyer belt schematic [*Gordon*, 1986]. It compensates the southward export of the North Atlantic Deep Water (NADW) formed in the sub-Arctic North Atlantic and plays an important role in the global ocean circulation and climate [*Beal et al*., 2011; *Caley et al*., 2012]. Recent studies have recognized that an increase in Agulhas leakage could strengthen the Atlantic overturning circulation in response to the poleward shift of the westerly jet in the Southern Hemisphere [*Biastoch et al*., 2009a; *Beal et al*., 2011; *Biastoch and Böning*, 2013]. The majority of Agulhas waters do not leak into the south Atlantic, but instead retroflect back into the Indian Ocean to form the Agulhas Return Current (ARC) [*Lutjeharms and Ansorge*, 2001], which flows eastward along the subtropical convergence zone and interacts with the local atmosphere [*Large and Yeager*, 2009]. The strong air-sea interaction is intimately linked to the Southern Annular Mode (SAM) [*Sallée et al*., 2010] and to the formation of the Sub-Antarctic Mode Water (SAMW) [*McCartney*, 1982; *Sallée et al*., 2006].

Because of the Agulhas waters' significant influence on the ocean circulation, mapping its pathways is crucially important. The interactions between the ACC and the subtropical convergence are essential for the exchange of water masses between the sub-Antarctic and subtropical zones of the Southern Hemisphere, but the path of the ARC and its interactions with the ACC are not well studied.

Here we use passive tracers integrated in a Southern Ocean State Estimate (SOSE) [*Mazloff et al*., 2010] to map the pathways of Agulhas water originating at 29°S. The results show that in addition to the Agulhas Leakage and the Agulhas Return Current, the Agulhas waters flow southeastward and enter the ACC at several mixing hot spots that are instigated by topographic obstacles. The most notable intrusion into the ACC occurs at the southwest Indian Ridge, the Crozet Plateau, and the Kerguelen Plateau (KP). The Agulhas waters also seem to play an important role in the formation of SAMW.

2. Methodology

2.1. The SOSE

The high-resolution (1/6° by 1/6°) SOSE has been used extensively in studying the Southern Ocean [*Mazloff et al*., 2010]. SOSE is constrained to a large number of observations, including satellite altimetry and Argo profiling floats. The solution is optimized by adjusting initial conditions, northern boundary conditions, and the atmospheric state. A restoring open boundary layer is present between 24.7°S and 26.7°S, where the velocity, temperature, and salinity are nudged to prescribed values. It has little effect on the Agulhas tracer transport as almost all the waters are transported southward at the beginning. SOSE investigations have included evaluations of current structures [*Firing et al*., 2011] and water mass transformation [*Cerovečki et al*., 2011, 2013], which are relevant to this study. The assimilation analyzed here is carried out for 3 years from 1 January 2008 to 31 December 2010. It is denoted Iteration 60 and available at sose.ucsd.edu.

2.2. The Agulhas Current System in SOSE

2.2.1. Horizontal Structure

The sea surface height (SSH) field in SOSE is comparable to that obtained from satellite data. Figure 1 shows the time-average and standard deviation of the SOSE SSH (right) and satellite derived mean dynamic topography [*Pavlis et al*., 2012] (DOT08) and standard deviation from AVISO (left) over the Agulhas current system regions for the SOSE period (2008–2010). Similar to the conclusion in *Griesel et al*. [2012], the mean dynamic topography in DOT08 is consistent with SOSE. The SSH is high in the South Indian Ocean, and also in a narrow band in the Southeast Atlantic Ocean delineating the mean pathway of the Agulhas leakage. Standing meanders are notable in the mean dynamic topography, indicating the effect of topographic steering on the Agulhas Return Current.

The standard deviation fields are similar in SOSE and AVISO. High SSH variability in both products occurs over the Retroflection region, the Agulhas Return Current, and the Southwest Indian Ridge (30°E, 50°S), downstream of the KP, and along the northward pathways that carries rings toward the Southeast Atlantic. The amplitude of the variability is slightly weaker in SOSE than in AVISO, but the structure is similar. Overall, SOSE produces an SSH field similar to that observed by satellite.

2.2.2. Vertical Structure

The Agulhas current in SOSE is similar in amplitude to previous studies and has a reasonable structure. The cross section of the mean meridional velocity at 32°S (Figure 2, left) shows a V-shape as observed [*Beal and Bryden*, 1999]. The core of the southward velocity exceeds 1 m s^{-1} centered about 60 km off the coast. The $1/6^{\circ}$ resolution in SOSE marginally resolves the narrow boundary current but does not fully represent the continental slope. As a result, the Agulhas undercurrent in SOSE is wider and less constrained to the continental slope than observations indicate.

2.2.3. Volume Transport

The transport of the Agulhas Current in SOSE, integrated along a zonal line at 32°S extending 204 km eastward from the coast, is consistent with observed values. The mean southward volume transport is 65.9 Sv (1Sv = 10^6 m^3 s^{-1}) with a standard deviation 14.6 Sv, and a 5 day mean maximum and minimum 105.5 and 34.7 Sv, respectively (Figure 3a). *Bryden et al*. [2005] estimated the 267 day averaged southward volume transport across 32°S to be 69.7 ± 21.5 Sv. SOSE has a northward undercurrent transport of 2.5 ± 2.1 Sv (Figure 3b), similar to the 2.7 ± 2.6 Sv Agulhas undercurrent in a 1/10° resolution nested-domain simulation by *Biastoch et al*. [2009b]. These model undercurrent transports are consistent but weaker than the 4.2 ± 2.9 Sv in *Bryden et al*. [2005] or the 4.2 ± 5.2 Sv in *Beal* [2009]. The Agulhas undercurrent transport in SOSE becomes 5.0 ± 4.8 Sv if integrated over 282 km from the coast. Both the northward and southward transports are highly modulated by intermittent eddies, and show little seasonal variability.

2.3. Experiments With Passive Tracers

Since our assessment of the Agulhas Current System in SOSE shows it to be consistent with observations, we carry out passive tracer experiments to map the pathways of the Agulhas waters. Passive tracers are released on 1 January 2008 as a pulse along 29°S between the South African continent and 42°E (yellow line in Figure 4). The section is chosen to be 11° wide in order to extend beyond the Agulhas Current and thus represents the greater Agulhas system. The sensitivity of our results to the tracer release initial

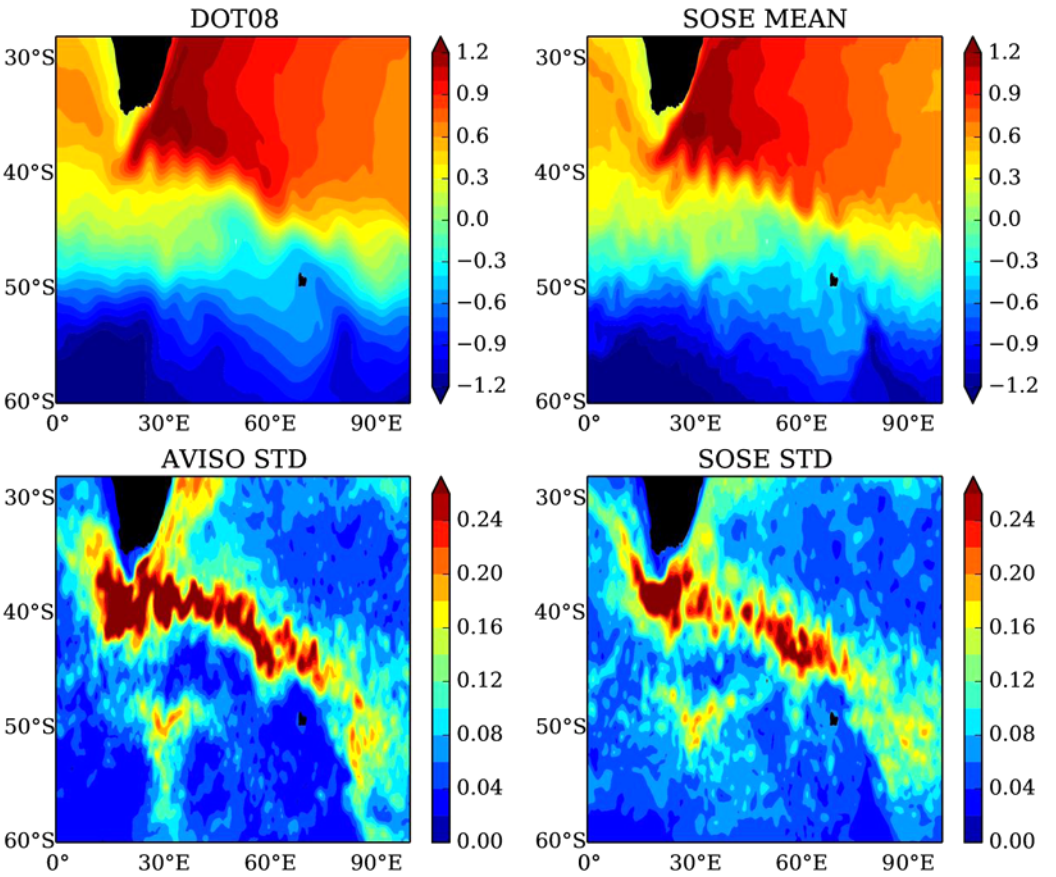

Figure 1. The mean dynamic topography (meter) from (top left) DOT08 [*Pavlis et al.*, 2012], and from the (top right) 3 year (2008–2010) SOSE solution. The standard deviation of SSH from the (bottom left) AVISO objectively mapped product and from the (bottom right) SOSE solution for 2008–2010.

condition is minimized both by releasing tracer at varying distances from the core of the Agulhas jet and by choosing initial conditions with a radius larger than the local eddy size or the width of the boundary current.

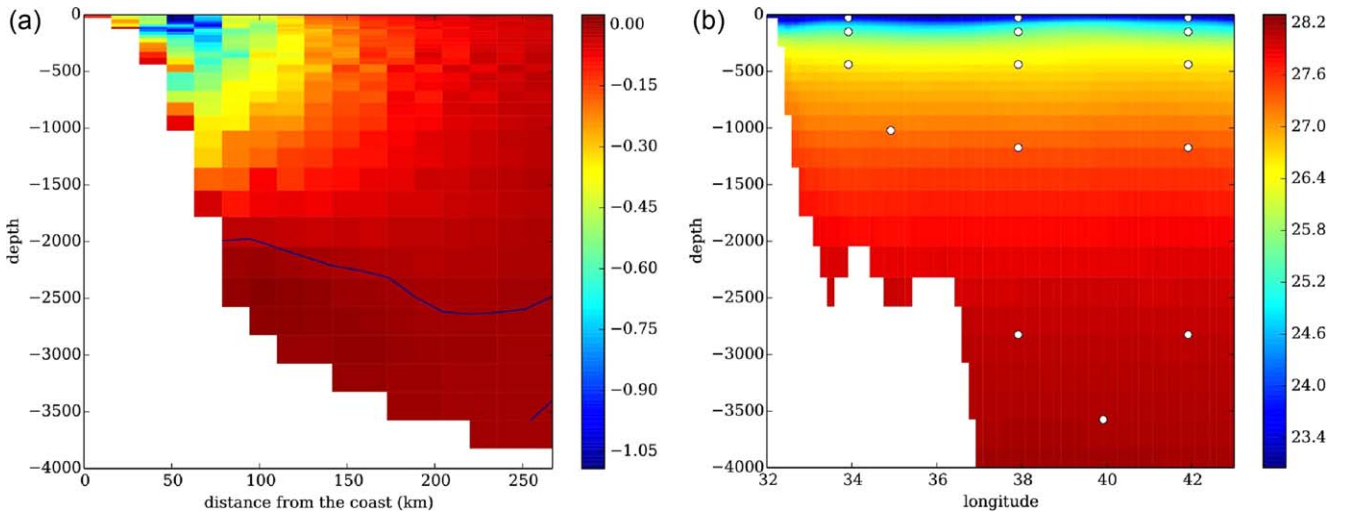

Figure 2. (left) The 3 year mean meridional velocity at 32°S. The line marks the zero velocity contour. (right) Section showing neutral density at 29°S from 32°E to 43°E. Tracer 1 fills the whole section. The centers of the other 15 localized tracers are marked by the white dots. Note that the latitude of the sections and the *x* axis is different in two figures.

In total, 16 tracers are used. Tracer 1 fills the entire section from surface to bottom (Figure 2, right). Another 15 localized tracer patches are simultaneously released within the same section to assess individual pathways of the water masses at different depths and offshore locations. Each of these 15 tracers is initialized by

$$c(x_0,y_0,z_k)=\begin{cases} A\cos\left(\pi\frac{x-x_0}{dx}+1\right)\cos\left(\pi\frac{y-y_0}{dy}+1\right)f(z|z_k) & x_0-dx<x<x_0+dx; \\ & y_0-dy<y<y_0+dy \\ 0 & \text{elsewhere} \end{cases}$$

$$f(z|z_k)=\begin{cases} 1/[\Delta z_{k-1},\Delta z_k,\Delta z_{k+1}] & z_{k-1}\le z\le z_{k+1} \\ 0 & \text{elsewhere}, \end{cases}$$

where in this case $dx=dy=1^\circ$ is chosen, and $A=1$ is chosen, though A can be an arbitrary value, and Δz_k represents the model layer thickness at the k_{th} vertical level. The tracers are advected online for 3 years from 2008 to 2010 as permitted by the SOSE duration. For this study, 3 years are sufficient, because after 3 years the Agulhas waters have been sufficiently modified such that they no longer retain their initial properties. The deep tracers are not transported southward within the 3 years studied, so are not discussed.

In order to quantify tracer transport, the SOSE domain is divided into nine sectors separated by the gray lines in Figure 4, i.e., the south, north, and interior of the ACC in the Atlantic, Indian, and Pacific Oceans. Here we choose the 20 and 140 Sv time-mean vertically integrated transport streamlines as proxies for the Polar Front (PF) and the Sub-Antarctic Front (SAF), and to delineate the southern and northern ACC boundaries. It may be optimal to define the fronts using instantaneous fields, but large uncertainties exist due to energetic eddies. We analyze the tracer budget based on the last year time-average which filters out the eddy fluctuations and expect the time-mean fronts to be more appropriate than instantaneous fronts for this analysis. By defining the SAF as the ACC boundary we only diagnose tracers that truly cross this front as being in the ACC, and exclude tracers that reside on the northern flank of the front. The specific choice of the ACC boundaries, however, does not affect the qualitative characteristics of the diagnosed tracer pathways. Transport streamlines are calculated by vertically integrating and then meridionally integrating the zonal velocity from south to north, with the zero streamline defined to be the Antarctic coast. The South Atlantic and South Indian are separated by the Good Hope line connecting the Cape of Good Hope and the 40°S parallel at 10°E. This line is often used in the calculation of the Agulhas leakage [e.g., *Richardson*, 2007; *Biastoch et al*., 2009a; *van Sebille et al*., 2010a]. The meridional line at 147°E connecting the Antarctic continent to Tasmania and Australia separates the South Indian and South Pacific oceans. By the end of the 3 year simulation less than 2% of tracer 1 has been lost through the northern boundary of the study domain in the Atlantic sector. Because the lost tracer cannot reenter the SOSE domain, we renormalize the tracer concentration at each time step in the analysis.

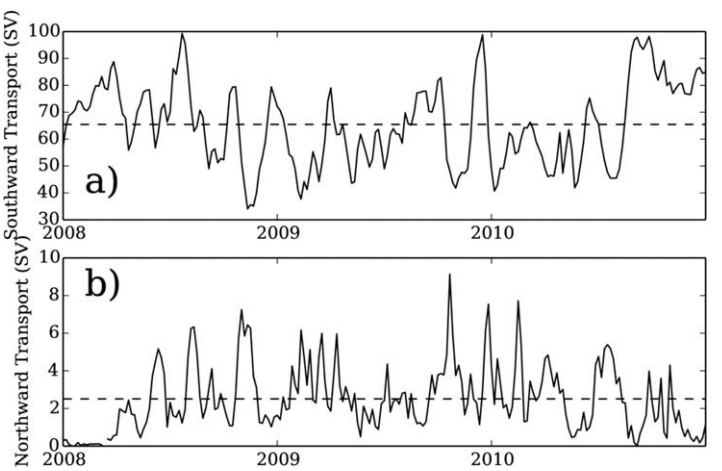

Figure 3. The time series of (a) southward and (b) northward transport integrated over 204 km off the coast at 32°S. 1 Sv = 10^6 m^3 s^{-1}.

2.4. Water Masses

Sections 4 and 5 discuss tracer distribution in terms of water masses including Sub-Antarctic Mode Water (SAMW), Southeast Indian SAMW (SEISAMW), Antarctic Intermediate Water (AAIW), and Indian Ocean Sub-Tropical Mode Water (IOSTMW). Here we follow the convention of *Talley et al*. [2011]. The associated temperature, salinity, and potential density for each water mass are listed in Table 1.

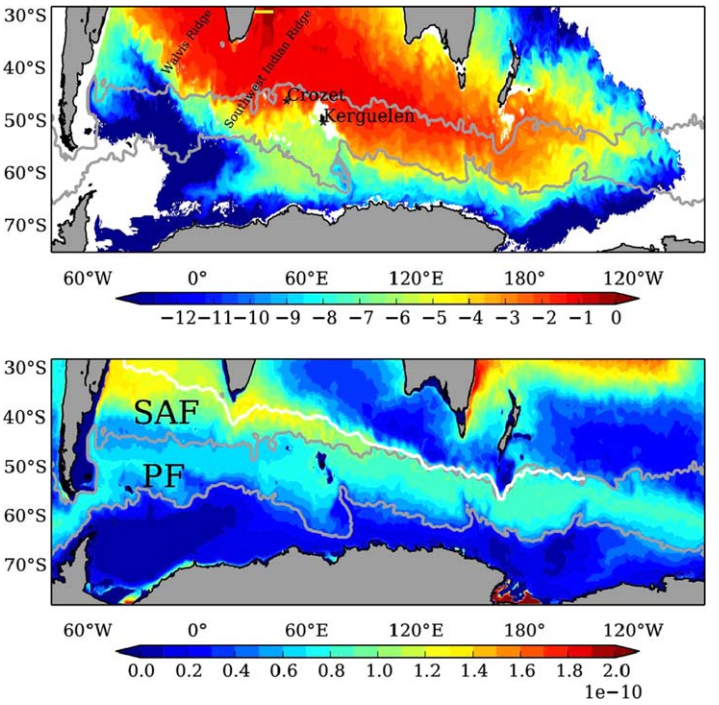

Figure 4. (top) The vertically integrated and time-averaged tracer content in a $\log_{10}$ scale (color) for the year 2010. The tracer is initially released in a band at 29°S within an 11° longitude range extending from the South African continent to 42°E (the yellow bar) and from the surface to the bottom. The gray lines divide the SOSE domain into nine sections. The more zonally oriented curved gray lines are vertically integrated transport streamlines: 20 Sv to the south and 140 Sv to the north. Thick white lines are the 3000 m isobath. (bottom) The potential vorticity ($f\rho^{-1}\partial\rho/\partial z$) at 500 m averaged over 3 years. The white line marks the main pathway of the intermediate tracer (around 500 m) as shown in Figure 7.

3. Horizontal Tracer Distribution

During the 3 year integration, the Agulhas waters are distributed broadly and reach all three ocean basins. Figure 4 shows the 2010 time-averaged tracer 1 concentration, integrated vertically, normalized by its maximum value and plotted on a logarithm scale. The core tracer pathway stretches from the northwest to the southeast following the Subtropical Front and the SAF through the Indian Ocean sector of the Southern Ocean. Figure 4 shows that the ACC fronts and topography play multiple roles in shaping the tracer pathways, acting as a barrier or as a mixer depending on the specific location. In sections 3.1–3.3, we describe the tracer distribution in the three ocean basins.

3.1. The South Atlantic Ocean

At the end of the 3 year integration, 9.9% of Tracer 1 has entered the South Atlantic Ocean. This is not the conventional fraction of the Agulhas Leakage as Tracer 1 samples a large area beyond the Agulhas Current. After entering the South Atlantic from the Agulhas Retroflection, the tracer is blocked from being advected further southwest first by the SAF (indicated by a significant drop in tracer content) and second by the mid-Atlantic Ridge at 0°E. The tracer is largely confined to the north of 51°S at 0°E. To the north of 40°S, however, steep topography, including the Walvis Ridge and the mid-Atlantic Ridge, play no detectable role in shaping the tracer pathways, as also noted in previous studies [*Boebel et al*., 2003; *Richardson*, 2007]. Some of the tracer reaches the east coast of South America and is transported poleward by the Brazil Current, subsequently crossing the SAF at the Brazil-Malvinas confluence.

3.2. The South Indian Ocean

At the end of 2010, 84.1% of tracer 1 remains in the south Indian Ocean north of the SAF and 5% has entered the ACC. Tracer concentration is high in the Mozambique Channel (around 40°E, 30°S), indicating the stagnant deep water in the channel. The Crozet Basin between the Southwest Indian Ridge and the Southeast Indian Ridge traps a large amount of tracer. The tracer is first mixed into the ACC around the Southwest Indian Ridge and the Crozet Plateau at (40°E, 45°S). A small portion of the mixed tracer passes the PF, enters the Enderby Basin and the Weddell Gyre around (40°E, 60°S), and travels westward along the Antarctic coast. A more significant cross-ACC transport occurs downstream of the KP at 70°E. The majority of this water is transported downstream

Table 1. Mode Waters Discussed in the Paper Following the Convention in *Talley et al*. [2011][a]

Acronym	Temperature (°C)	Salinity (psu)	Potential Density (kg m^{-3})
SAMW	4–15	34.2–35.8	26.5–27.1
SEISAMW	8	34.55	26.8
AAIW	4.7	34.39	27.2
IOSTMW	17–18	35.6	26.0

[a]The listed water masses are sub-Antarctic mode water (SAMW), southeast Indian SAMW (SEISAMW), Antarctic intermediate water (AAIW), and Indian Ocean subtropical mode water (IOSTMW).

within the ACC. This striking cross-ACC transport is consistent with the finding of a uniform potential vorticity pool downstream of the KP [*Thompson et al*., 2010], caused by enhanced eddy induced mixing. The tracer content decreases sharply to the south of the PF.

3.3. The South Pacific Ocean

By the end of the 3 year integration, 1% of Tracer 1 has entered the South Pacific. The tracer is confined to the north of the PF. This is especially clear to the south of Tasmania (near 150°E, 60°S), where both the PF and the tracer pathway are deflected by the Southeast Indian Ridge. High tracer content straddles the SAF, which does not appear to be a barrier to Agulhas waters because of the tracer mixing into the ACC upstream of the KP.

3.4. The Effect of Kerguelen Plateau

As a further demonstration of the significance of the topographic effect, we plot a Hovmöller diagram of the vertical profile of the tracer concentration at five locations up and downstream of the KP (Figure 5). Upstream of the KP (Figure 5a) tracer crosses the ACC only 5 times during the 3 year period with a very short duration in each event. This means that, although infrequent, the tracer can be advected into this region by sporadic eddies.

Immediately upstream of the KP (Figure 5b), one significant tracer intrusion event occurs around month 24, i.e., 2 years after the tracer release. One notable feature is the deep tracer near 1000 m. This deep tracer is not a result of the local subduction of the upper-level tracer, because tracer appears much earlier in the deeper layer (at month 19) than in the upper layer (at month 23). The tracer concentration shows long persistence with small temporal variability, indicating that the tracer is transported from the north/northwest to this location by the mean boundary current along the western boundary of the plateau. The tracer that appears around 1300 m during the second half of the third year may also have been advected from the north/northwest upstream. Low concentration of tracer is found on the KP shelf due to the surface Ekman transport being northward (Figure 5c).

In contrast to the region upstream of the KP (Figures 5a and 5b), tracer appears much more frequently and with a much larger concentration downstream (Figures 5d and 5e). Tracer released near the surface requires 15 months to reach the region downstream of the KP, while the transit time for tracer released deeper is longer. The tracer transport appears to be more intermittent at site d than at site e, suggesting that the tracer at site d is brought by eddies but that the tracer has been homogenized before reaching site e. Among the five sample sites, the largest tracer concentration occurs at site e, downstream of the KP.

4. Vertical Tracer Distribution

Pathways differ by density class and cannot be studied solely from a uniform surface-to-bottom tracer release. Hence we also analyzed the 15 additional tracers that were released in localized positions. Their depths and longitudes are indicated by the pie charts in Figure 6. Over the 3 year simulation more than 60% of the waters in the Agulhas system remain in the South Indian Ocean north of the ACC (IN), and for deep water originating in the Mozambique Channel almost 100% remains in IN (Figure 6, IN). Intermediate waters originating between 400 and 1500 m are more readily transported out of the Indian Ocean than were the surface waters. This is especially true for water originating close to the African continent. Up to 28% of intermediate water enters the South Atlantic Ocean (AN), and about 12% ends in the Indian sector of the ACC (IA). As surface water is advected faster than deep waters, most of the tracer that ends in the Pacific was released in the upper ocean. The partition is relatively independent of the offshore distance, which corroborates the results of *van Sebille et al*. [2010b].

Based on water mass properties and horizontal distributions, we split the tracers shown in Figure 6 into three groups. The surface tracer refers to the ensemble of the upper six tracers (0–400 m), the intermediate tracer refers to the middle six tracers (400–1500 m), and the deep tracer refers to the deep three tracers. The deep tracers are not transported southward so are not discussed further.

The vertically integrated surface and intermediate tracer contents are shown in Figures 7a and 7b. The white lines are the mean tracer pathways defined as the tracer first moment in *y*,

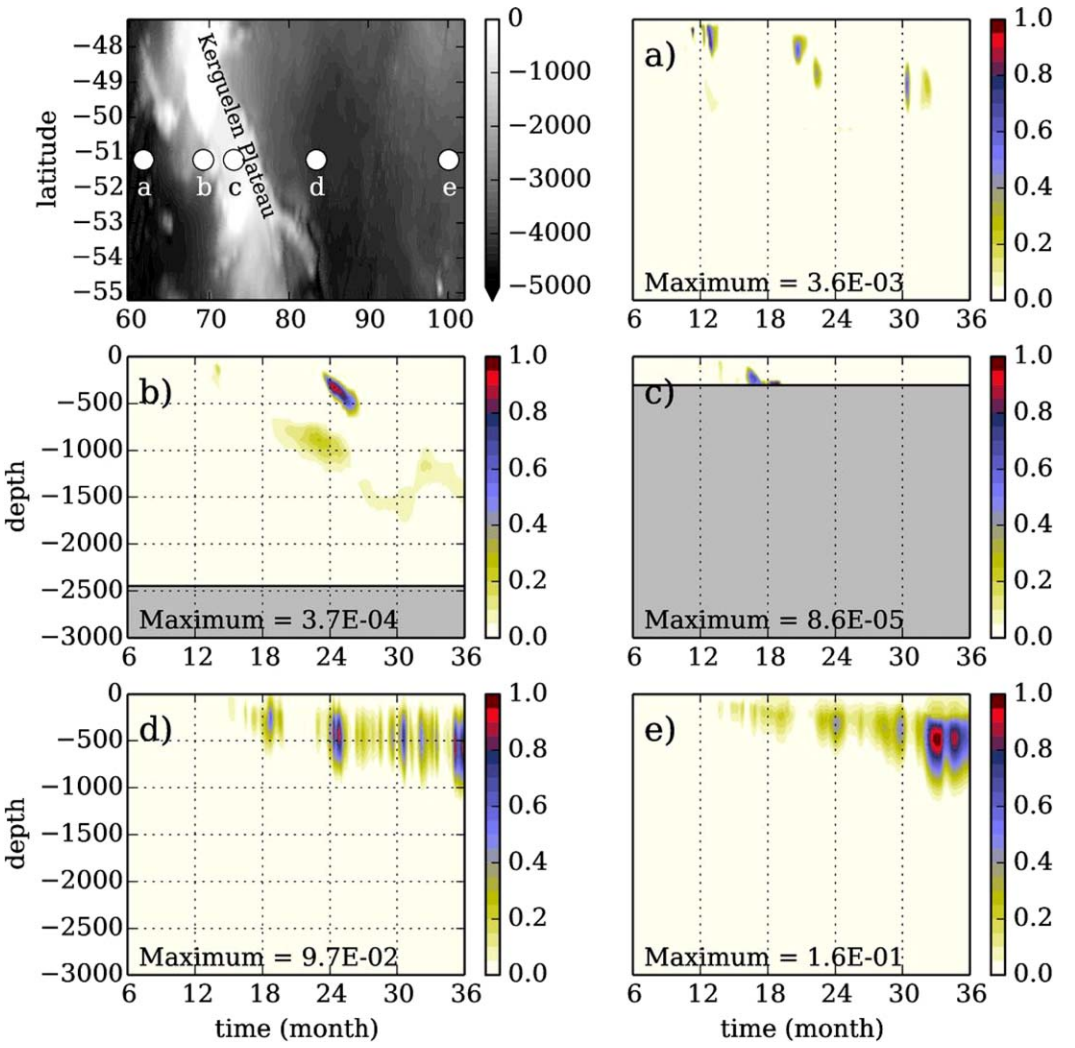

Figure 5. (top left) The depth of the ocean bottom for the region over the KP. The white dots mark five locations for which the Hovmöller diagram of the vertical profile of the tracer concentration is shown in plots a–e. The tracer concentration in each plot is normalized by the maximum value noted at the bottom. The levels below seafloor are shaded gray.

$$y_c = \frac{\int y \langle c \rangle^{z,t} dy}{\langle c \rangle^{y,z,t}}, \tag{1}$$

where we use the angle brackets to represent integration, i.e., $\langle c \rangle^{z,t} = \int \int c dz dt$. The surface and intermediate tracer distributions share a qualitatively similar large-scale feature with a northwest-southeast tilt. The main surface pathway is shifted northward relative to the main interior pathway due to surface northward Ekman flow (compare the relative shift of the two white lines to the location of the SAF in Figures 7a and 7b).

The properties of the vertical tracer distribution are measured by the first moment, A_c, and the second moment, σ_A, with respect to a chosen variable A,

$$A_c(x, y, t) = \frac{\langle Ac \rangle^z}{\langle c \rangle^z} \tag{2}$$

and

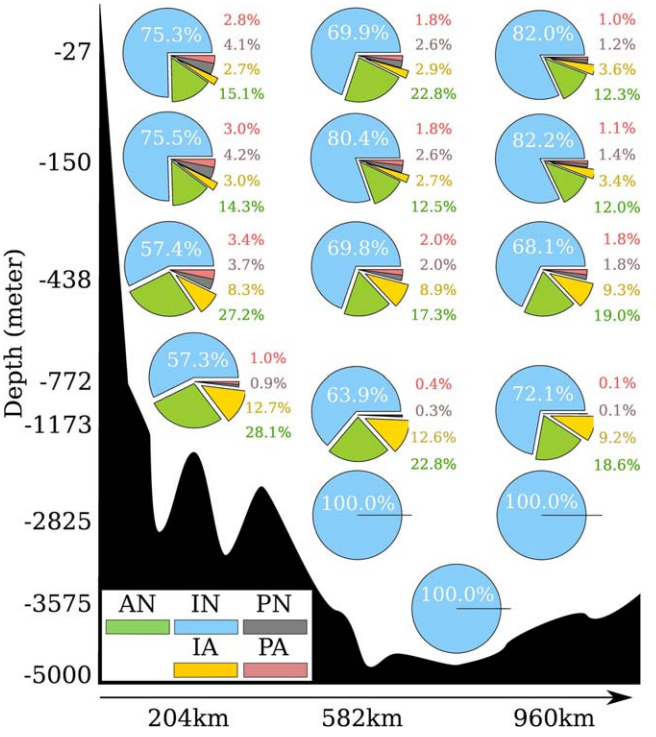

Figure 6. Final tracer distributions into five main ocean sectors (color-coded) for 15 initial Gaussian tracer patch releases, represented by pie charts, at different depths (*y* axis) and offshore locations (*x* axis). The ocean sectors are denoted as AN, IN, PN to represent sections north of the ACC in the Atlantic, Indian, and Pacific Oceans, respectively. The IA and PA denote the ACC in the Indian Ocean and Pacific Ocean, respectively. The depth-coordinate is stretched to accommodate all the pie charts.

$$\sigma_A^2(x,y,t)=\frac{\langle c(A-A_c)^2\rangle^z}{\langle c\rangle^z}.$$

The first and second moments represent the local center and thickness of a specific tracer in *A* space. For example, if *A* represents the vertical coordinate *z*, the first moment represents the tracer mean depth and the second moment represents the tracer spread in the vertical.

Figure 7 shows the first moment of the surface (c, e, and g) and intermediate (d, f, and h) tracer in depth (c and d), neutral density (e and f), and salinity (g and h) space averaged over the last year. The results are organized and presented for three different regions, i.e., the South Atlantic, the South Indian Ocean to the north of the ACC (IN), and the Indian Ocean sector of the ACC (IA).

4.1. The Main Pathway in the Indian Ocean

By the end of the 3 year model integration, the surface tracers have drifted northward, carried by the surface Ekman flow. As a result, there is less surface tracer than intermediate-level tracer within the Retroflection region (Figures 7a and 7b). The surface tracer deepens to about 300 m along the pathway in the Indian Ocean sector. The deepening over the southeast Indian region coincides with the deep mixed-layer region, suggesting that the tracer is mixed downward by the winter deep convection.

The main pathway going through the deep mixed-layer region indicates that waters are modified, or preconditioned, by air-sea fluxes as they travel along the Agulhas Return Current to the SAMW pool. The tracer gradually becomes denser (Figure 7e) and fresher (Figure 7g) along this southeastward pathway, eventually contributing to the SAMW formation via lateral advection. Upon reaching the location where the SEISAMW is found vertical mixing spreads the tracer over a thicker depth range (Figure 8a), making it more uniform in density (Figure 8c).

Tracers initiated in intermediate layers (Figure 7d) enter the Agulhas region at deeper levels than the surface tracers (Figure 7e), but the intermediate-level tracers gradually rise as they move toward the south Pacific. Intermediate tracers are advected mostly along isopycnals indicated by the constant density along the main pathway (Figure 7f). The main pathway of the intermediate tracers merges with the SAF to the east of 80°E, meaning that the SAF does not inhibit cross-frontal exchange. As a result of cross-frontal exchange intermediate tracers become less saline as they move southeastward along the main pathway (Figure 7f). By the time they reach the southeast Indian Ocean, surface and intermediate tracers share the same depth and density ranges, suggesting that both contribute to the SAMW formation.

The surface-originating tracers are found to the north of the SAF over the southeast Indian Ocean (Figure 7c), while intermediate tracers straddle the SAF (Figure 7d). This is because most of the surface tracers are constrained to the north of the SAF and become well mixed in the pool of SAMW, while the core of the intermediate tracers coincides with the SAF (Figure 9). As a result, the surface tracers occupy a thick depth range along the main pathway, but they are compact in density space (Figures 8b and 9). For the

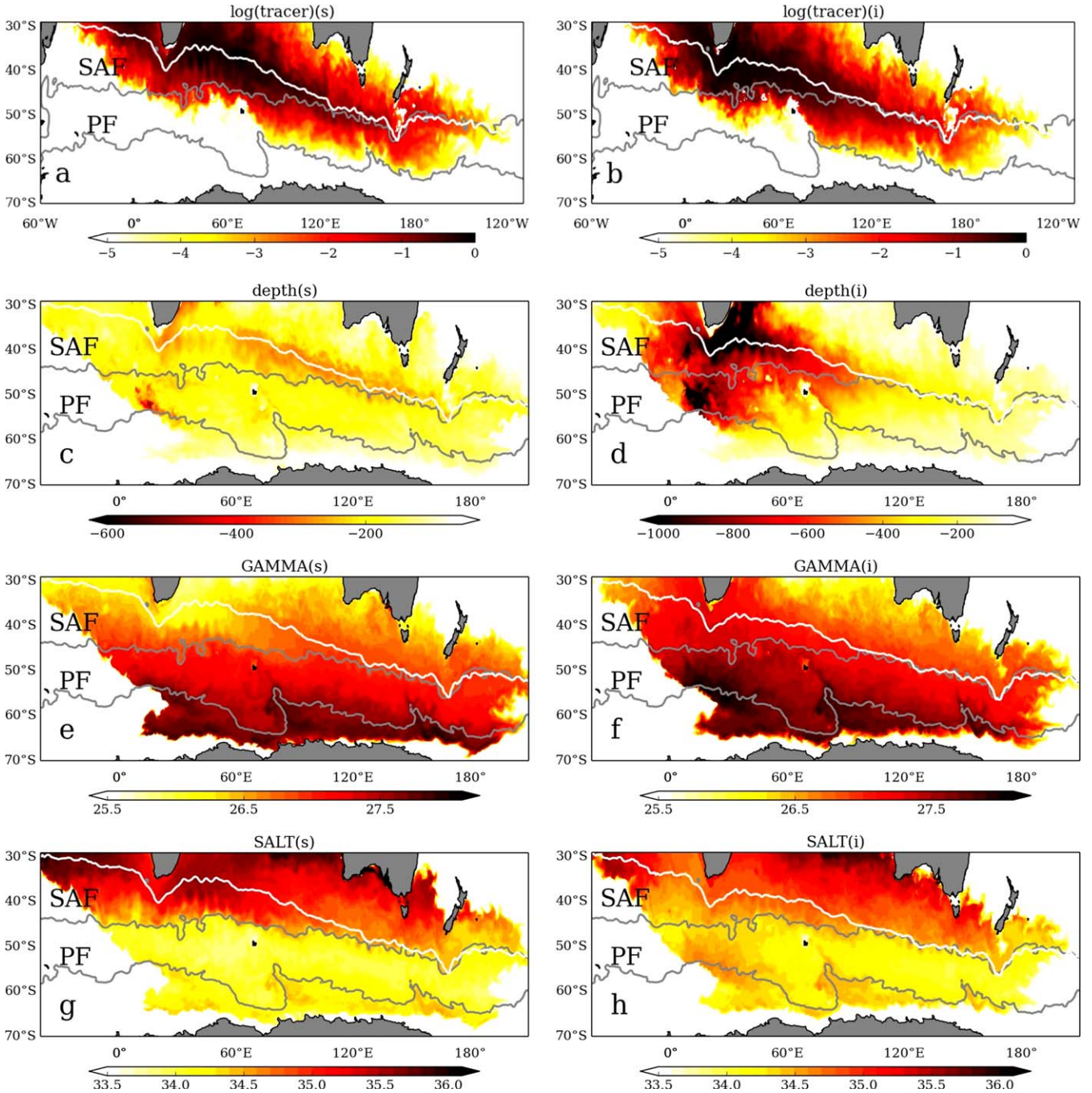

Figure 7. The (a) surface and (b) intermediate tracer concentrations averaged for the final year plotted on a logarithmic scale. The white lines mark the main tracer pathways for the intermediate tracer and surface tracer defined by y_c in equation (1). The center of the surface and intermediate (c and d) tracer depth, (e and f) neutral density, and (g and h) salinity. Two gray lines are the same as in Figure 4 denoting SAF and PF.

intermediate tracers, the lack of an obvious cross-SAF gradient downstream of the KP suggests that SAF and the associated eddies act as a blender to stir intermediate waters across the front (Figures 8b and 9). As shown in Figure 9, both the surface and intermediate tracers contribute to the SAMW within the southeast Indian Ocean.

4.2. The South Atlantic Ocean

The tracers are advected into the South Atlantic and remain north of the SAF for both the surface and intermediate levels (Figures 7a and 7b). The main pathways defined by the first moment in *y* extend

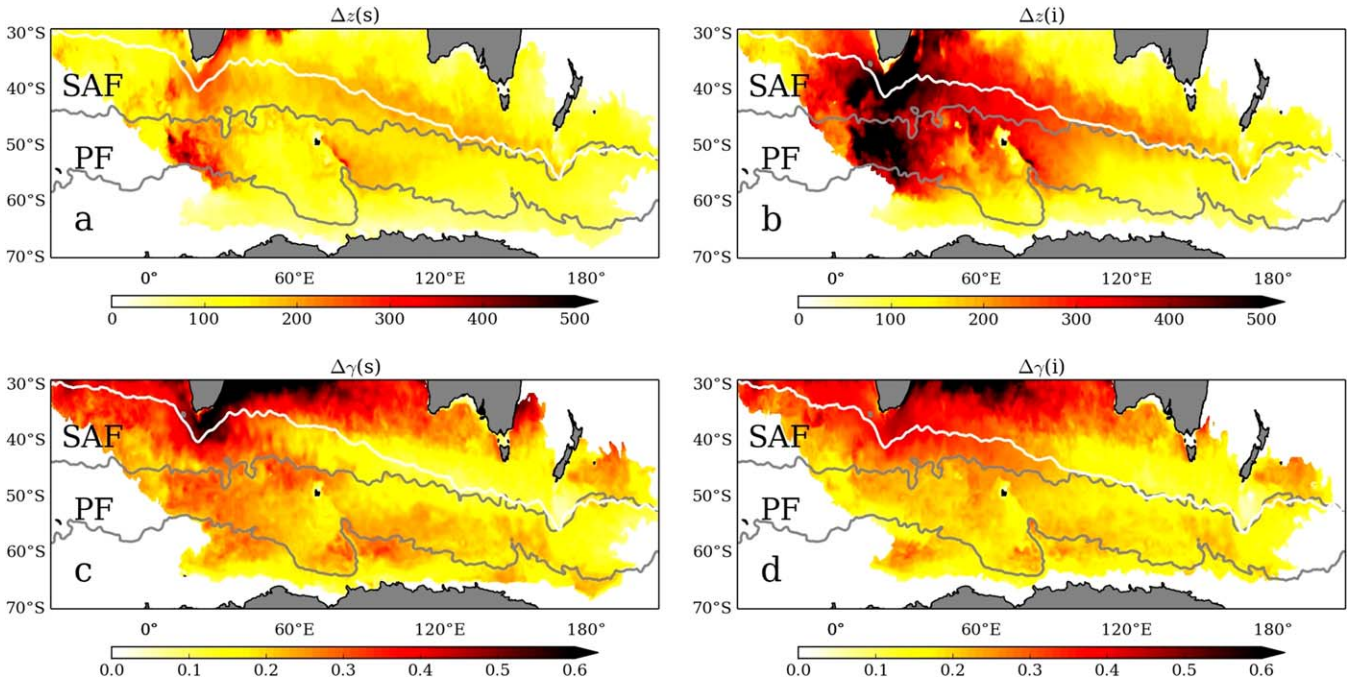

Figure 8. The (a and c) surface and (b and d) intermediate tracer thickness in depth (meter) (Figures 8a and 8b) and density (kg m^{-3}) space (Figures 8c and 8d). The white and gray lines are the same as in Figure 7.

northwestward suggesting the pathway of the Agulhas Leakage as previously discussed [*Richardson*, 2007]. After entering the South Atlantic, both surface and intermediate tracers shoal (Figures 7c and 7d) due to the shallower isopycnals in the South Atlantic Ocean. The tagged waters also become denser (Figures 7e and 7f) due to the surface cooling over the retroflection region (Figure 10) and eddy induced mixing with ambient Atlantic waters, and less saline (Figures 7g and 7h). The large tracer spread in density space in the South Atlantic Ocean (Figures 8c and 8d) is a continuation of the large spread in the South Indian recirculation region, indicating that the tracers have been extensively mixed before entering the South Atlantic Ocean.

4.3. Cross-Frontal Transport

Tracer intrusion into the ACC primarily occurs downstream of the KP. Some intrusions, however, are also apparent at the Crozet Plateau region (Figures 7a and 7b). Over this Crozet Plateau region, the surface tracer content drops sharply to the south of the SAF, indicating that local fronts block the southward advection of surface tracers. The stream function-based SAF approximately matches the tracer contour, suggesting that the SAF acts as a barrier over this region. Note, however, that the true barrier may be one of several strong fronts that exist in the region, including the Crozet Front [*Pollard and Read*, 2001]. In addition, the Polar Front can sometimes extend further north in this region [*Orsi et al*., 1995; *Belkin and Gordon*, 1996].

Nevertheless some tracer does enter the ACC in this region, with intermediate depth tracers being more readily mixed into the ACC than surface tracers (Figure 7b). This tracer intrusion occurs at several hot spots, i.e., the southwest Indian ridge where interbasin exchange was observed previously [*Pollard and Read*, 2001] and the deep channel between the Crozet Islands and the Kerguelen (Figures 8a and 8b). Once these tracers enter the ACC they mix, becoming denser and moving deeper in the water column (Figures 7c–7f). The stark meridional contrast in the tracer density and depth indicates that tracers have entered the deeper layers of the ACC. Some of these tracers are then advected downstream of the KP through, the Fawn Trough and they then flow along the southern ACC boundary (Figures 7c–7f, 8a, and 8b). The cross-KP flow through the Fawn Trough is a well-observed feature [*Roquet et al*., 2009].

One caveat, however, is that the tracer content is low within this region resulting in large uncertainties in the quantification of this pathway. Nevertheless, the results point out an interesting cross-front exchange process and confirm the importance of the southwest Indian Ridge in interbasin exchanges.

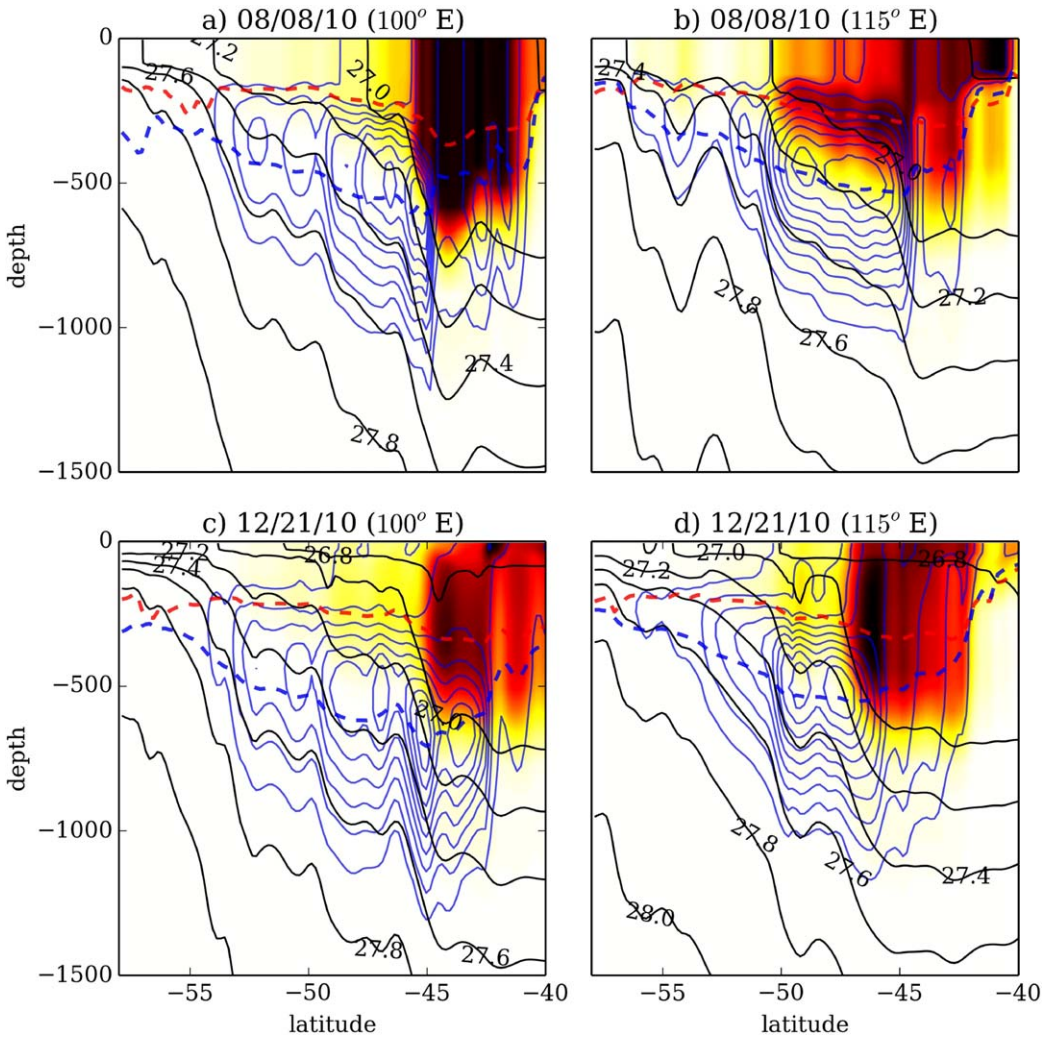

Figure 9. Cross sections of the 5 day averaged concentration of a surface tracer (color) and an intermediate tracer (blue contour) along (a and c) 100°E and (b and d) 115°E during 8 August 2010, the austral winter (Figures 9a and 9b), and 21 December 2010, the austral summer (Figures 9c and 9d). The black contours show the instantaneous neutral density (kg m^{-3}). The dashed lines mark the first moment in *z* for the surface (red) and intermediate (blue) tracers. The approximate latitudes of the (SAF, PF) defined by the temperature front at 200 m (thresholds: 2.5°C for the PF and 6°C for the SAF) are (48°S, 53°S), (50°S, 57°S), (49°S, 54°S), and (51°S, 57°S), for Figures 9a–9d, respectively. Note that large uncertainties exist due to the distortion of isotherms by instantaneous energetic eddies.

Downstream of the KP the tracers are first transported into the ACC by a train of eddies that emerge from the SAF to the north of the Plateau at 70°E (refer to the video in the supporting information). The majority of the tracers remain to the north of the PF. At the end of the 3 year run the surface-originating tracer that remains in the ACC is still shallower than about 300 m (Figure 7c). This tracer is now found largely in a pool of water with neutral density around 27.0 ± 0.2 (Figure 7e) especially during austral winter time which is marked by the red-black color in Figures 9a and 9b), and it clearly shows an upper-layer salinity front (Figure 7g).

Tracers originating at intermediate depths are transported southeastward mainly by the ACC primarily along the core of the SAF, as suggested by the coincidence of the tracer concentration maximum and the SAF (Figure 9 blue contours). To the north of the SAF, tracers are mixed into the mode water pool, indicated by the vertical homogenization of tracers across density levels. To the south of the SAF, tracers are advected along isopycnals indicated by the similar shape of tracer contours and isopycnals. The coincidence of the local maximum in tracer concentration with warm-core eddies (the local deepening in isopycnal contours) is a sign that eddies are involved in the southward and upward transport of tracer, as discussed in the residual mean formulation [*Marshall and Speer*, 2012, and the references therein].

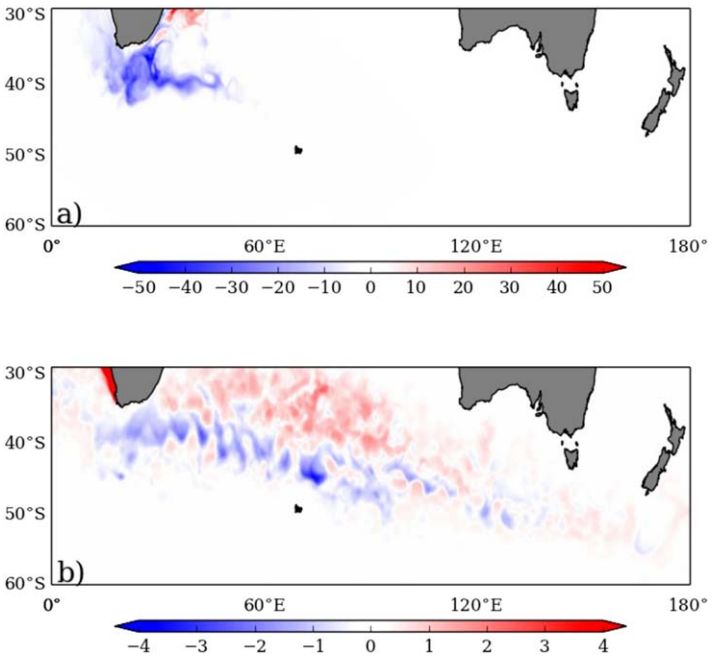

Figure 10. The net surface heat flux (W m^{-2}) experienced by Tracer 1 during (a) the first 7 months and (b) the last 12 months. Negative values represent ocean heat loss.

The phenomenon of tracer being advected to the south and mixed to the north of the SAF is consistent with the regional potential vorticity (Figure 4, bottom). Downstream of the KP, the main pathway of the intermediate tracers merges with the SAF and bisects the low potential vorticity pool of the SEISAMW and the higher potential vorticity ACC water. The tracers north of the main pathway are modified and blended into the low potential vorticity pool. That they originated as high potential vorticity waters means they counteract the mode water formation processes. Meanwhile, the lack of mixing of tracers south of the SAF allows persistence of the high potential vorticity signature. Furthermore, this pathway points to the importance of waters originating in the Agulhas Current in explaining the relatively high potential vorticity signature found over much of the ACC.

To summarize, the main pathways of the Agulhas waters are oriented along a northwest to southeast axis. Surface initialized tracers are shifted northward relative to intermediate depth initialized tracers because of surface Ekman transport. West of 80°E, the pathways are centered north of the SAF. The SAF acts as a barrier upstream of the KP blocking direct tracer mixing into the ACC from the subtropical region, with an exception of the southwest Indian ridge and the deep channel between the Crozet Islands and the KP where tracers leak into the ACC at depth. Downstream of the KP (east of 80°E), the SAF acts as a blender, mixing tracers into the ACC. A significant amount of Agulhas waters reach the SEISAMW formation region. Before reaching this area, surface waters experience strong surface cooling within the Agulhas Retroflection and the Agulhas Return Current regions (Figure 10). In contrast intermediate waters remain approximately on the same isopycnal. Both processes strongly suggest the importance of lateral advection and preconditioning of the Agulhas waters to facilitate the SEISAMW formation.

5. Water Mass Modification

Agulhas waters are transformed as they spread, as is also observed in other modeling studies [e.g., *van Sebille et al*., 2010a]. Here we use the tracers to mark the Agulhas waters and study their evolution. The first question is how quickly the Agulhas waters transform. Water mass transformation is reflected in the heat and salt content of the waters marked by the tracers. We use the tracer-weighted potential temperature, a proxy for tracer heat content, to investigate the time scale of water mass transformation,

$$\theta_c(t) = \frac{\langle \theta c \rangle^{x,y,z}}{\langle c \rangle^{x,y,z}},$$

where θ is potential temperature referenced to 0 pressure. The true heat content of a tracer is

$$H_c(t) = \rho c_p \langle c \rangle^{x,y,z} \theta_c(t),$$

where c is tracer concentration, ρ density, c_p the specific heat capacity for sea water, and H_c the tracer heat content. The tendency of the tracer temperature consists of two parts

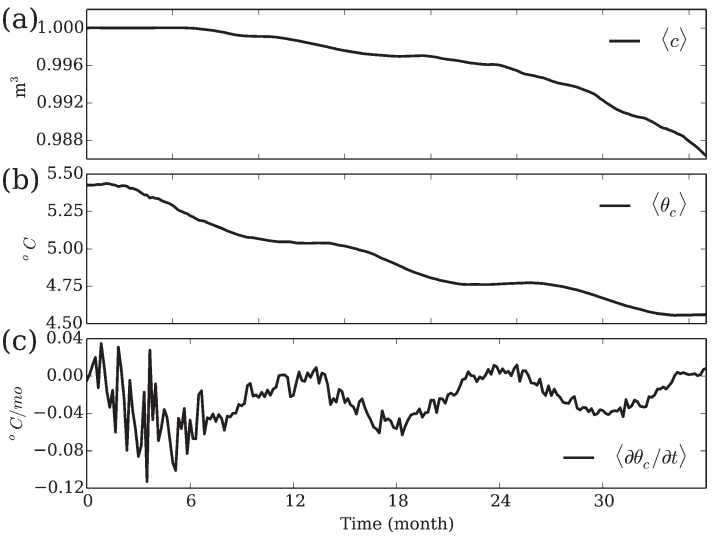

Figure 11. The evolution of tracer content normalized by (a) the initial value, (b) tracer temperature (in °C), (c) time tendency of the tracer temperature °C/month.

$$\frac{\partial \theta_c}{\partial t}\langle c\rangle^{x,y,z} = \left\langle c\frac{\partial \theta}{\partial t}\right\rangle^{x,y,z} + \left\langle \theta\frac{\partial c}{\partial t}\right\rangle^{x,y,z}.$$

The first term on the right-hand side represents the influence of the temperature change of the water parcel marked by tracers. The second term represents the change due to the tracer spreading into different temperature ranges. For instance, if a tracer is stagnant, then $\partial c/\partial t = 0$, and the change of the tracer-weighted temperature is solely due to the heat in and out of the tracer marked waters by surface forcing or diffusion. Similarly, if a temperature field is stationary, the tracer temperature change is solely because the tracer spreads into regions with different temperatures. In our case both make measurable contributions.

We calculate the evolution of the tracer temperature based on Tracer 1 (Figure 11). The total tracer volume is conserved within 98.8% (plot a). The 1.2% is lost through the northern boundary. The tracer-weighted temperature continuously decreases (plot b), due to the initial high potential temperature of the Agulhas waters. Most of the water mass modification happens during the first 7 months, after which the tracers quasi-equilibrate with the ambient atmosphere and ocean. Subsequent changes are due primarily to air-sea flux as indicated by the clear seasonal cycle in $\partial\theta_c/\partial t$ (plot c).

We use the other 15 tracers to analyze the evolution of different water masses in T-S space (Figure 12). Near-surface Agulhas waters transform quickly as they flow southward. The tropical surface waters originating at potential density level 23.5 kg m^{-3} (referenced to the surface and following the standard procedure of subtracting 1000 kg m^{-3}) are transformed to a density of 25.5 kg m^{-3} in less than 6 months (thick red in Figure 12a). These waters continue to become denser, reaching a potential temperature of 14–15°C, salinity of 35.3–35.4, and potential density of 26.2–26.3 kg m^{-3} (red dots in Figure 12f). At this density, the water is consistent with a mixture of IOSTMW and SAMW [*Beal et al*., 2006; *Cerovečki et al*., 2013]. The quick initial transformation of the surface water is primarily caused by surface heat loss as the temperature decreases sharply (Figure 12f red), but the salinity is relatively unchanged. Mixed-layer dynamics play a role in evolving the waters in the upper 500 m, and the seasonal cycle is apparent in Figures 12a–12c.

The tracer released at 438 m has an initial potential density of 26.6 kg m^{-3}, potential temperature 13.2°C, and salinity of 35.3. This water freshens and cools as it flows adiabatically southeastward, indicating an interior along-isopycnal mixing with the ACC waters.

Intermediate waters originating at 772 m initially have a potential density of 27.3 kg m^{-3} (Figure 12d, thick purple), but quickly mix with upper-layer waters becoming warmer and saltier. They enter the ARC with a potential density of approximately 27.0 kg m^{-3} and then flow adiabatically southeastward and experience little change in properties. They do, however, become slightly colder and fresher indicating some along-isopycnal mixing with ACC waters.

The intermediate Agulhas waters that reach the ACC (Figures 12e and 12f) experience large mixing amplified by eddies generated from topographically induced instabilities. The waters have density 26.5 kg m^{-3} upon entering the ACC, and eventually cool and freshen, so that they can be characterized as AAIW. Meanwhile, deep waters initialized in the Agulhas Current below 2000 m are relatively stagnant (black dot in Figure 12f).

All waters that enter the South Atlantic experience dramatic transformations (thin lines in Figures 12a–12d and dots in Figure 12g). The Agulhas surface waters travel for about 2 months before reaching the Agulhas

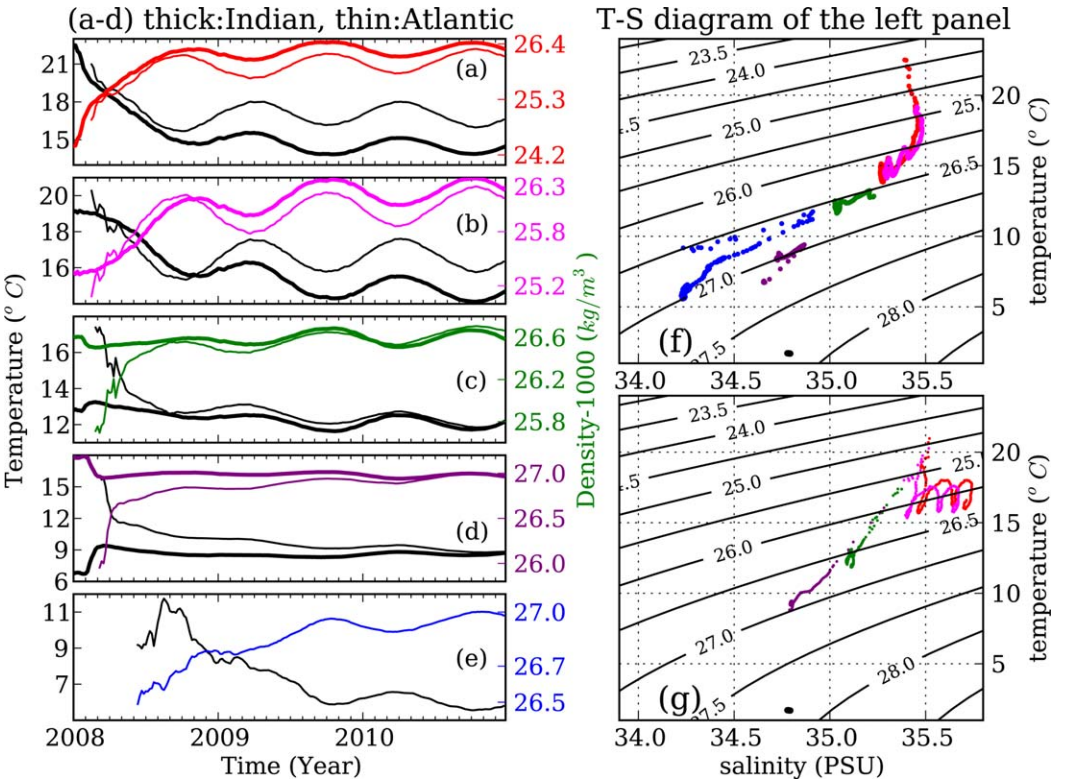

Figure 12. Evolution of four water masses (color-coded consistently in all plots) shown as (left) time series and (right) in a potential temperature-salinity diagram. (a–d) Tracers initially released at 27, 150, 438, and 772 m, respectively. Colored lines represent tracer-weighted density, and black lines potential temperature. The thick lines in Figures 12a–12d represent tracer found in the Indian Ocean north of the ACC, and the thin lines represent tracer found in the South Atlantic north of the ACC. (e) Tracer-weighted density (blue) and temperature (black) in Indian sector of the ACC. The right plot shows the same data but in a T-S diagram. (f and g) The thick dots and thin dots in Figures 12a–12d, respectively. The blue dots in Figure 12f correspond to the blue line in Figure 12e. In addition, the tracer released around 2825 m is shown in the right plot with black dots. These dots cluster at (34.8, 1.7°C) indicating the stagnation of that water mass.

Bank and entering the South Atlantic (Figures 12a and 12b). These waters mix with subsurface waters and evolve for about a year until reaching a point where they begin to oscillate around a density of approximately 26 kg m^{-3} (Figures 12a, 12b, and 12g). The intermediate waters become warmer and saltier after entering the South Atlantic Ocean (Figures 12c and 12g) due to strong turbulent mixing with upper waters at the retroflection region and upwelling in the Benguela Current (figure not shown).

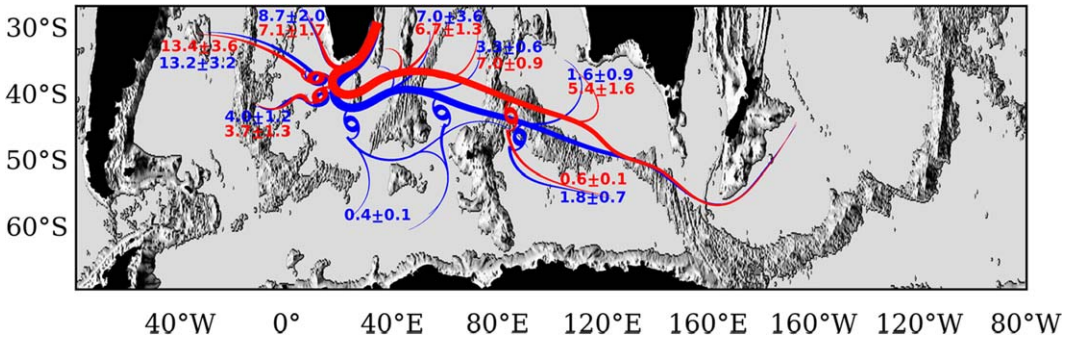

Figure 13. A schematic of the Agulhas water pathways. Bathymetry is in black-gray colors. Red color represents the tracers released in the upper layer of the Agulhas Current (the upper 400 m). The blue colors represent the intermediate tracers released between 400 and 1500 m. Numbers show the ensemble-averaged percentage of the tracer in each subdomain branch averaged in 2010 with standard deviation as uncertainties. The remaining percentage, 56.1% for the surface tracers and 60% for the intermediate tracers, still resides in the main pathway. Spirals represent the location of enhanced stirring, inferred by large variations in properties. The main pathway of the tracer is meridionally shifted between surface and intermediate layer, which is due to the northward surface Ekman flow. Refer to Appendix A for details on the creation of this schematic.

Based on a detailed subdomain diagnoses of the tracer content in year 2010 and on the evolution of tracer transport during the 3 year simulation (detailed in Appendix A) we infer a schematic (Figure 13) showing the pathway of Agulhas waters over two main levels, surface (0–400m, red) and intermediate (approximately 400–1500m, blue). The main pathways of the Agulhas water at these two levels show a clear meridional offset, with the surface waters shifted equatorward due to the northward Ekman transport. Hot spots of cross-frontal transport of Agulhas waters, which exist in both levels but are more prevalent in the intermediate level, occur at the retroflection region, the Southwest Indian Ridge, and the Agulhas, Crozet and KPs. Most of the cross-ACC tracer mixing occurs at these hot spots, with the location downstream of Kerguelen being the most significant. A small amount of tracer crosses the Polar Front and is advected toward the Antarctic Shelf.

6. Summary

The Agulhas Current system transports heat and salt from the Indian Ocean into the South Atlantic and Southern Oceans. In this study, less attention has been paid to the effect of the Agulhas leakage which is extensively discussed elsewhere [*Beal et al*., 2011, and the references therein]; instead, we focus on the southeast pathways of Agulhas waters and find that the contributions of the Agulhas waters to the SEISAMW and the ACC water are not negligible.

Using SOSE we carry out a series of passive tracer experiments initialized within an 11° wide zonal section at 29°S to map the pathways of water originating in the Agulhas current system. For the last year of the 3 year run, we find that the majority (from 60% to 100% depending on specific water mass) of the Agulhas waters stay in the South Indian Ocean north of the SAF, 10–28% enter the South Atlantic Ocean through the boundary current along Africa and via Agulhas rings in the retroflection region. Up to 12% of Agulhas Current intermediate water enters the ACC in the South Indian Ocean.

Significant amounts of Agulhas waters are advected into the SEISAMW formation region. The surface waters experience strong surface cooling before reaching the southeast Indian Ocean, but the intermediate waters are transported along isopycnals while transforming into the SEISAMW. This emphasizes the importance of lateral advection in the SEISAMW formation.

Eddies and topography play an important role in water mass exchange between ocean sectors. "Hot spots" of exchange are associated with major seamounts. Enhanced cross-ACC transport occurs around the Agulhas and Crozet Plateaus and particularly just downstream of the KP. The exchange downstream of the KP is so great that "hot spots" of mixing that are further downstream, such as the Macquarie Ridge and the Campbell Plateau, become insignificant for redistributing the tracers originating in the Agulhas current. The fraction of Agulhas waters transported into and across the ACC is small compared with the Agulhas current transport itself; however, the accumulated modest transport of Agulhas waters toward Antarctica could have significant climatic implications as the heat and salt gradients between the subtropics and the polar oceans are substantial.

Appendix A: Quantification of Pathway Branches

Quantification of pathway branches is accomplished by dividing the domain into 16 sectors based on the position of the two main pathways (white lines in Figure 7), the mean SSH streamlines, and two meridional lines separating the Atlantic, Indian, and Pacific Ocean basins. Refer to Figure A1 for the structure and specific values used for defining the 16 sectors. The ensemble mean of the percentage of tracer content entering each sector is presented in Figure 13. The ensemble standard deviation is also given as an estimate of the uncertainty. The uncertainty estimate is approximate due to the limited ensemble size of six releases, but serves as an adequate guideline. The numbers given in Figure 13 represent the pathway branches deemed most important for meridional property redistribution. Numbers for the Pacific are omitted due to the fact that after the 3 year simulation they are insignificant. Numbers for the mean pathway are omitted as they are sensitive to the choice of the sector bounds.

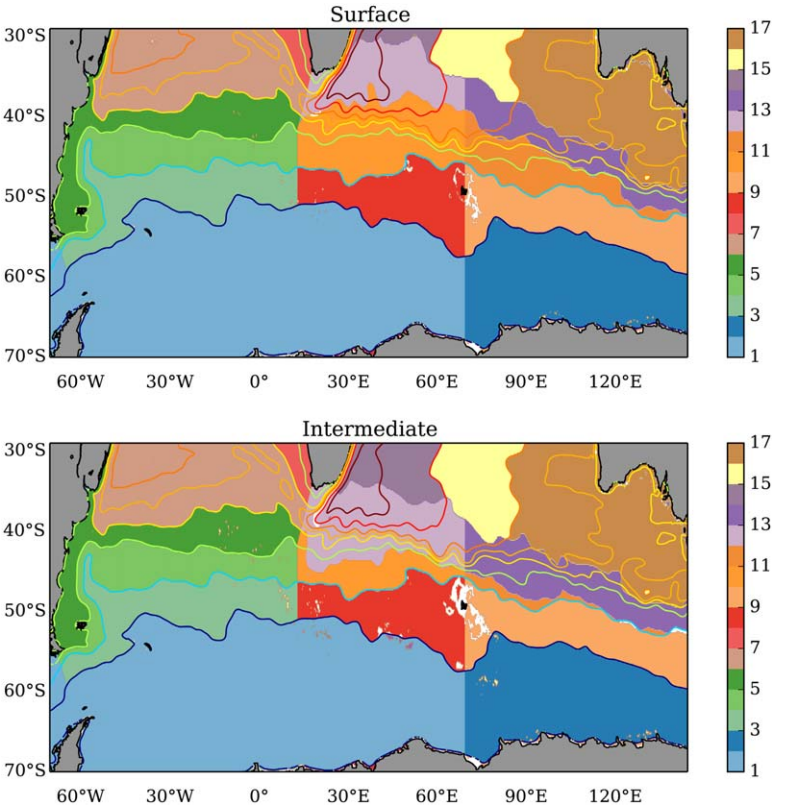

Figure A1. Color-coded 16 sectors used in quantifying the tracer pathways shown in Figure 13. (top) The surface layer releases and (bottom) the intermediate layer releases with the primary difference being in the location of the main pathway. The contours show the 3 year averaged SSH. The SSH contour levels are [−0.8, −0.2, 0.2, 0.4, 0.5, 0.6, 0.8, 1.0] starting from south. The levels −0.8 and −0.2 m approximate the 20 and 140 Sv vertically integrated transport streamlines and denote the boundaries of the main ACC core. Regions 12 and 13 are the main tracer pathways shown in Figure 7, divided by the 70°E meridian crossing the KP. The time-averaged tracer budget in 2010 is quantified for these 16 sectors and presented schematically in Figure 13.

Acknowledgments

We acknowledge the National Science Foundation (NSF) for support of this research through grants OCE-1234473 and OPP-0961218. SOSE was produced using the Extreme Science and Engineering Discovery Environment (XSEDE), which is supported by National Science Foundation grant MCA06N007. We thank Lynne Talley and Ivana Cerovečki for helpful conversations. Comments from two reviewers and Veronica Tamsitt helped improve the manuscript. The data used in this study are available at sose.ucsd.edu.

References

Beal, L. M. (2009), A time series of Agulhas Undercurrent transport, *J. Phys. Oceanogr.*, *39*(10), 2436–2450, doi:10.1175/2009JPO4195.1.

Beal, L. M., and H. L. Bryden (1999), The velocity and vorticity structure of the Agulhas Current at 32S, *J. Geophys. Res.*, *104*(C3), 5151–5176, doi:10.1029/1998JC900056.

Beal, L. M., T. K. Chereskin, Y. D. Lenn, and S. Elipot (2006), The sources and mixing characteristics of the Agulhas Current, *J. Phys. Oceanogr.*, *36*(11), 2060–2074, doi:10.1175/JPO2964.1.

Beal, L. M., W. P. M. De Ruijter, A. Biastoch, and R. Zahn (2011), On the role of the Agulhas system in ocean circulation and climate, *Nature*, *472*(7344), 429–436, doi:10.1038/nature09983.

Belkin, I. M., and A. L. Gordon (1996), Southern Ocean fronts from the Greenwich meridian to Tasmania, *J. Geophys. Res.*, *101*(C2), 3675–3696, doi:10.1029/95JC02750.

Biastoch, A., and C. W. Böning (2013), Anthropogenic impact on Agulhas leakage, *Geophys. Res. Lett.*, *40*, 1138–1143, doi:10.1002/grl.50243.

Biastoch, A., and W. Krauss (1999), The role of mesoscale eddies in the source regions of the Agulhas Current, *J. Phys. Oceanogr.*, *29*(9), 2303–2317.

Biastoch, A., C. W. Böning, F. U. Schwarzkopf, and J. R. E. Lutjeharms (2009a), Increase in Agulhas leakage due to poleward shift of Southern Hemisphere westerlies, *Nature*, *462*(7272), 495–498, doi:10.1038/nature08519.

Biastoch, A., L. M. Beal, J. R. E. Lutjeharms, and T. G. D. Casal (2009b), Variability and coherence of the Agulhas Undercurrent in a high-resolution ocean general circulation model, *J. Phys. Oceanogr.*, *39*(10), 2417–2435, doi:10.1175/2009JPO4184.1.

Boebel, O., J. Lutjeharms, C. Schmid, W. Zenk, T. Rossby, and C. Barron (2003), The Cape Cauldron: A regime of turbulent inter-ocean exchange, *Deep Sea Res., Part II*, *50*(1), 57–86, doi:10.1016/S0967-0645(02)00379-X.

Bryden, H. L., L. M. Beal, and L. M. Duncan (2005), Structure and transport of the Agulhas Current and its temporal variability, *J. Oceanogr.*, *61*(3), 479–492, doi:10.1007/s10872-005-0057-8.

Caley, T., J. Giraudeau, B. Malaizé, L. Rossignol, and C. Pierre (2012), Agulhas leakage as a key process in the modes of quaternary climate changes, *Proc. Natl. Acad. Sci. U. S. A.*, *109*(18), 6835–6839, doi:10.1073/pnas.1115545109.

Cerovečki, I., L. D. Talley, and M. R. Mazloff (2011), A comparison of Southern Ocean air-sea buoyancy flux from an ocean state estimate with five other products, *J. Clim.*, *24*(24), 6283–6306, doi:10.1175/2011JCLI3858.1.

Cerovečki, I., L. D. Talley, M. R. Mazloff, and G. Maze (2013), Subantarctic mode water formation, destruction, and export in the eddy-permitting Southern Ocean state estimate, *J. Phys. Oceanogr.*, *43*(7), 1485–1511, doi:10.1175/JPO-D-12-0121.1.

Firing, Y. L., T. K. Chereskin, and M. R. Mazloff (2011), Vertical structure and transport of the Antarctic Circumpolar Current in Drake Passage from direct velocity observations, *J. Geophys. Res.*, *116*, C08015, doi:10.1029/2011JC006999.
Gordon, A. L. (1986), Interocean exchange of thermocline water, *J. Geophys. Res.*, *91*(C4), 5037–5046, doi:10.1029/JC091iC04p05037.
Griesel, A., M. R. Mazloff, and S. T. Gille (2012), Mean dynamic topography in the Southern Ocean: Evaluating Antarctic Circumpolar Current transport, *J. Geophys. Res.*, *117*, C01020, doi:10.1029/2011JC007573.
Harris, T. (1972), Sources of the Agulhas current in the spring of 1964, *Deep Sea Res. Oceanogr. Abstr.*, *19*(9), 633–650, doi:10.1016/0011-7471(72)90091-5.
Large, W. G., and S. G. Yeager (2009), The global climatology of an interannually varying air-sea flux data set, *Clim. Dyn.*, *33*, 341–364, doi:10.1007/s00382-008-0441-3.
Lutjeharms, J., and I. Ansorge (2001), The Agulhas Return Current, *J. Mar. Syst.*, *30*(1–2), 115–138, doi:10.1016/S0924–7963(01)00041-0.
Lutjeharms, J. R. E. (1976), The Agulhas Current System during the northeast monsoon season, *J. Phys. Oceanogr.*, *6*(5), 665–670.
Marshall, J., and K. Speer (2012), Closure of the meridional overturning circulation through Southern Ocean upwelling, *Nat. Geosci.*, *5*(3), 171–180, doi:10.1038/ngeo1391.
Mazloff, M. R., P. Heimbach, and C. Wunsch (2010), An eddy-permitting southern ocean state estimate, *J. Phys. Oceanogr.*, *40*(5), 880–899, doi:10.1175/2009JPO4236.1.
McCartney, M. S. (1982), The subtropical recirculation of mode waters, *J. Mar. Res.*, *40*, 427–464.
Orsi, A. H., T. Whitworth, and W. D. Nowlin (1995), On the meridional extent and fronts of the Antarctic Circumpolar Current, *Deep Sea Res., Part I*, *42*(5), 641–673, doi:10.1016/0967-0637(95)00021-W.
Pavlis, N. K., S. A. Holmes, S. C. Kenyon, and J. K. Factor (2012), The development and evaluation of the Earth Gravitational Model 2008 (EGM2008), *J. Geophys. Res.*, *117*, B04406, doi:10.1029/2011JB008916.
Pollard, R. T., and J. F. Read (2001), Circulation pathways and transports of the Southern Ocean in the vicinity of the Southwest Indian Ridge, *J. Geophys. Res.*, *106*(C2), 2881–2898, doi:10.1029/2000JC900090.
Richardson, P. L. (2007), Agulhas leakage into the Atlantic estimated with subsurface floats and surface drifters, *Deep Sea Res., Part I*, *54*(8), 1361–1389, doi:10.1016/j.dsr.2007.04.010.
Roquet, F., Y.-H. Park, C. Guinet, F. Bailleul, and J.-B. Charrassin (2009), Observations of the Fawn Trough Current over the Kerguelen Plateau from instrumented elephant seals, *J. Mar. Syst.*, *78*(3), 377–393, doi:10.1016/j.jmarsys.2008.11.017.
Sallée, J.-B., N. Wienders, K. Speer, and R. Morrow (2006), Formation of Subantarctic Mode Water in the southeastern Indian Ocean, *Ocean Dyn.*, *56*(5–6), 525–542, doi:10.1007/s10236-005-0054-x.
Sallée, J.-B., K. G. Speer, and S. R. Rintoul (2010), Zonally asymmetric response of the Southern Ocean mixed-layer depth to the Southern Annular Mode, *Nat. Geosci.*, *3*(4), 273–279, doi:10.1038/ngeo812.
Talley, L. D., G. L. Pickard, W. J. Emery, and J. H. Swift (2011), *Descriptive Physical Oceanography: An Introduction*, 6th ed., 560 pp., Elsevier, Boston.
Thompson, A. F., P. H. Haynes, C. Wilson, and K. J. Richards (2010), Rapid Southern Ocean front transitions in an eddy-resolving ocean GCM, *Geophys. Res. Lett.*, *37*, L23602, doi:10.1029/2010GL045386.
van Sebille, E., P. J. van Leeuwen, A. Biastoch, and W. P. de Ruijter (2010a), Flux comparison of Eulerian and Lagrangian estimates of Agulhas leakage: A case study using a numerical model, *Deep Sea Res., Part I*, *57*(3), 319–327, doi:10.1016/j.dsr.2009.12.006.
van Sebille, E., P. J. van Leeuwen, A. Biastoch, and W. P. M. de Ruijter (2010b), On the fast decay of Agulhas rings, *J. Geophys. Res.*, *115*, C03010, doi:10.1029/2009JC005585.